This manuscript is a preprint and has not been peer reviewed. The copyright holder has made the manuscript available under a Creative Commons Attribution 4.0 International (CC BY) license and consented to have it forwarded to EarthArXiv for public posting.

# Future hydrology of a Himalayan basin shaped by elevation dependent shifts in water balance components

Pranisha Pokhrel[1], Philip D. A. Kraaijenbrink[2], Jasper Griffioen[1,3], Thom A. Bogaard[4], Walter W. Immerzeel[2],

**1** Copernicus Institute of Sustainable Development, Utrecht University, 3584 CB, Utrecht, The Netherlands
**2** Department of Physical Geography, Utrecht University, 3584 CB, Utrecht, The Netherlands
**3** TNO Geological Survey of the Netherlands, 3584 CB, Utrecht, the Netherlands
**4** Department Water Management, Delft University of Technology, 2600 GA, Delft, The Netherlands

* p.pokhrel@uu.nl

## Abstract

Mountainous basins in the Himalayas serve as critical "water towers" sustaining downstream livelihoods, yet their hydrological response to climate change is complex due to extreme elevation gradients. This study investigates the future hydrology of the Karnali basin (situated in Western Nepal) by disaggregating water balance components along its elevation profile. Using the fully distributed hydrological model SPHY forced by five CMIP6 climate models under three emission scenarios (SSP1-2.6, SSP3-7.0, and SSP5-8.5), simulations were conducted for mid century (2041–2070) and late century (2071–2100) periods relative to a 1991–2020 reference. Projections indicate a warmer and wetter future, with mean annual precipitation increasing by 19% to 38% and temperatures rising by 1.5 °C to 5.1 °C by the late century. A widespread shift from snowfall to rainfall is projected, with the most significant declines in snowfall fraction occurring between 2,000 and 4,000 m. While total annual discharge at the basin outlet is projected to increase by 35% to 59% by 2100, this masks a critical internal reorganization of the water balance. Snowmelt contributions are projected to decline and peak up to 43 days earlier under high-emission scenarios, reducing water yield in climate sensitive zones between 3,000 and 5,000 m. These losses are offset by substantial increases in rainfall runoff and baseflow at lower elevations, specifically between 1,000 and 2,000 m. This elevation dependent shift transforms the basin into a more rainfall dominant system, weakening its natural buffering capacity and increasing sensitivity to precipitation variability. These findings suggest heightened risks of hydrological extremes and highlight the necessity of elevation based analysis to capture the spatial redistribution of water components in mountainous basins.

## Introduction

Mountain ranges are often referred to as "water towers" because they naturally store and supply fresh water that sustains downstream environmental ecosystems and human livelihoods [1, 2]. The water stored in snow, glaciers and the soil is gradually released over time to sustain the river flow and support the water security. Mountainous water

This manuscript is a preprint and has not been peer reviewed. The copyright holder has made the manuscript available under a Creative Commons Attribution 4.0 International (CC BY) license and consented to have it forwarded to EarthArXiv for public posting.

resources therefore play a critical role for irrigation, hydropower, livelihood and ecosystems downstream including protected areas and national parks. The Karnali River basin is an example of such a basin. The Karnali River basin, one of Nepal's largest, originates from the Tibetan Plateau and the High Himalaya, flows through the hills to the lowlands before becoming a major tributary of the Ganges River system. The river flow from Karnali basin is vital for maintaining downstream water availability and supporting livelihood within this transboundary region.

Climate change is expected to substantially alter the hydrology of the mountainous basins through interconnected processes. Future projections suggest an intensification of the water cycle, as evapotranspiration and precipitation will increase and alter their variability with warming temperatures [3]. The mountain regions are also likely to experience cryospheric changes, including a reduction in snow storage, the timing of snowmelt, glacier retreat, and permafrost degradation [3]. In High Mountain Asia, several studies consistently project an increase in precipitation in combination with a declining snow cover and a change in glacier melt under future climate conditions [2,4–9]. One of the direct consequences of warming is a shift in precipitation phase from snow to rain. As a larger fraction of precipitation falls as rain rather than snow, the direct rain runoff will increase on the expense of the slower snowmelt. Consequently, the day to day variability becomes larger, river runoff becomes less predictable and the peak flow may occur earlier in the season. The seasonal snow storage is likely to be reduced and this will alter the seasonal distribution of melt water. Simultaneously, higher temperatures may enhance the glacier melt in the short term but it will be reduced over time due to glacier retreat. At the same time warmer conditions and higher water availability due to increased precipitation can enhance evapotranspiration, and impact the runoff coefficient and water availability. These conspiring climate change effects can have broad hydrological consequences including changes in total and seasonal discharge, shifts in the timing, increased risk of hydrological extremes, and weakening of the basin's natural buffering capacity, as highlighted in several studies [9–13].

All of the impacts described above are strongly elevation dependent. Lower elevations may be impacted more by rainfall and evapotranspiration, elevations near the freezing temperature line may be most sensitive to changes in snowfall fraction, and the highest elevations may continue to receive substantial contributions from snow and glacier melt. The total discharge change in the basin is consequence of water balance components redistribution across the elevation zones. An elevation based study of water components is important to understand how climate change will affect the discharge of the basin. The future hydrology of mountainous basins like Karnali is sensitive to climate change, where seasonal water availability depends on both rainfall and delayed meltwater contributions. Winter and early spring runoff in the Karnali basin are strongly influenced by snow accumulation and melt in the upper catchment. Previous studies have documented the impact of future climate change in western Nepal and Karnali basin [14–18]. These studies consistently project warming across western Nepal river basins with higher precipitation and river discharge. The study by [18] predicts the magnitude flood to increase up to 79% by the end of the century under high emission scenario and also become more frequent compared to historical period. However, these studies use basin or sub-basin scale models and even with distributed models, the results quantify the overall aggregated response of the basin to climate change for long term water availability. To fully understand hydrological changes, it is important to understand the spatial connectivity between the water cycle changes from the High Himalaya to the downstream Terai, the flat low lying belt along the southern foothills of Nepal.

In this study, we bridge the gap by disaggregating the response of the basin to climate change by analyzing hydrological data along the elevation gradient of the basin.

This manuscript is a preprint and has not been peer reviewed. The copyright holder has made the manuscript available under a Creative Commons Attribution 4.0 International (CC BY) license and consented to have it forwarded to EarthArXiv for public posting.

We use a fully distributed hydrological model to analyze how climate change reshapes the future hydrology of the Karnali basin. Given that climate changes are expected to alter both total water availability and the seasonal water storage, and release, we first assess the overall future changes at basin scale before examining how specific water balance components vary across elevation zones. This allows us to analyze how climate induced changes in high elevations interact with the hydrological processes in the low elevation zone allowing a comprehensive understanding of water redistribution across the gradient. Specifically, this study focuses on three major questions: a) How does climate change affect the precipitation amount and its phase across the elevation range in the Karnali basin? b) How will the water balance components vary with elevation in the future for Karnali basin? and c) How do these elevation dependent changes influence the total magnitude and seasonal timing of the discharge at the outlet of Karnali basin?

## Study area

The Karnali River drains an area of 45,496 $km^2$ from the high Himalayas to the lowland plains and spans an elevation gradient from 186 to 7,606 m above mean sea level. Along the north-south transect of Karnali basin, the landscape can be divided into five distinct physiographic zones (see fig 1A): the Terai ($< 200$ m), Siwalik Hills (750–1500 m), Middle Mountains (1500–2500 m), High Mountains (2200–4000 m), and High Himalayas ($> 4000$ m) [19, 20]. Beyond the High Himalayas lies the Tibetan Plateau. These physiographic zones are characterized by distinct topography, land cover and contribute differently to the overall water balance of the basin.

The upper basin is dominated by grassland, sparse vegetation, and snow/glacier cover, whereas the lower basin consists mainly of forests, together with croplands and urban areas [21]. Overall, forest and grassland account for 48% and 32% of the basin area, respectively.

Over the period 1991–2022, the basin average annual precipitation (P), actual evapotranspiration ($ET_A$), and total discharge ($Q_{Tot}$) were 1485, 574, and 914 mm $yr^{-1}$, respectively [21]. Precipitation in the Karnali basin is strongly dominated by the summer monsoon months (JJAS), which contributes about 70% of the annual total, while winter precipitation (DJF), associated with the westerlies, contributes around 9%. Topography plays a dominant role in controlling the precipitation pattern in the basin [22, 23]. Most of the precipitation in the Karnali basin is concentrated between 1–2 km elevation. At elevations above 5 km, the precipitation declines and the Tibetan Plateau is the driest and located in the rain shadow.

Evapotranspiration also varies strongly with elevation. At lower elevations ($<2$ km), where forest and agricultural land dominates and moisture availability is relatively high, potential evapotranspiration ($ET_P$) reaches about 2470 mm $yr^{-1}$, while actual evapotranspiration ($ET_A$) reaches its maximum value of about 1336 mm $yr^{-1}$. Long-term average daily temperature decreases from about 23 °C in the 1 km to 2 km elevation band to about $-4$ °C in the 7 km to 8 km elevation band.

The total discharge ($Q_{Tot}$) in the basin consists of rain runoff ($Q_{RR}$), baseflow ($Q_{BF}$), snowmelt ($Q_{SM}$) and glacier melt ($Q_G$). The Karnali basin is mostly rainfed, with rainfall runoff contributing 40% of the total discharge. Snowmelt is also substantial and contributes 24% of the basin runoff. Glacier melt provides minor contribution (0.8%) to the basin runoff [21]. The main contribution from $Q_{RR}$ is concentrated in the $<2$ km elevation range where precipitation is highest (Fig 1B). $Q_{SM}$ is generated mainly from elevations above 3 km. The contributions are strongly controlled by the basin hypsometry, as winter snow accumulated below 5 km primarily drives winter and pre-monsoon discharge, whereas snow accumulated above 5 km mainly contributes to the discharge during the monsoon season [21]. Seasonal snow storage acts as a buffer

This manuscript is a preprint and has not been peer reviewed. The copyright holder has made the manuscript available under a Creative Commons Attribution 4.0 International (CC BY) license and consented to have it forwarded to EarthArXiv for public posting.

and delays runoff to the snowmelt season.

The basin hypsometry (Fig. 1B) indicates that a large proportion of the basin area is concentrated in the Middle and High Mountains. In total, 36% of the basin area lies between 2–4 km, 26 % between 4–5 km and 17 % between 5–6 km. In contrast, only 1% of the basin area is situated above 6 km. This distribution highlights the importance of Middle and High Mountains in controlling the basin's hydrological response as these are the zones where seasonal snow accumulates and is stored. The large elevation gradient, strong spatial variability in climate, and substantial fraction of basin area at different elevation zones make the basin sensitive to climate change.

**Fig 1. Conceptual overview Karnali basin and water balance components.** A) The schematic cross-section of the Karnali basin along an elevation transect from the Terai to the Tibetan plateau. The transect represents a mean elevation profile across 21 transects from South (low elevation) to North (high elevation) along the Karnali basin. The long-term average value of main water balance components for the reference period are also provided. B) The panel shows the location of the study basin within the Ganges river system and the DEM of the Karnali basin. C) Annual water fluxes $km^3\,yr^{-1}$ by 500 m elevation band for the reference period, showing precipitation, actual evapotranspiration, and total discharge with its components shown as stacked filled areas. Circles to the left of each elevation band indicate the relative area of that band, while circle color represents the long-term mean air temperature ($T_{avg}$).

# Materials and methods

## Hydrological model

To simulate future hydrological impacts, we use the Spatial Processes in Hydrology (SPHY) model. SPHY is a fully distributed water balance model that simulates snow and glacier processes at an intermediate level of detail [24]. The model also includes the full hydrological cycle, including rainfall runoff, evapotranspiration, and soil processes. SPHY has been frequently applied in the hydrological modeling of large to small scale mountainous river basins [5, 6, 8, 25–27]. The SPHY model was used previously to simulate the Karnali basin for the reference period 1991-2022 with a spatial resolution of $500 \times 500$ m at a daily time step. For the reference period, the model uses downscaled ERA5 reanalysis data [28] as gridded forcing, which includes daily precipitation and daily minimum, maximum, and mean temperatures. The total discharge generated at an outlet by the SPHY model is the sum of its discharge components: the surface runoff ($Q_{RR}$), snowmelt discharge ($Q_{SM}$), glacier melt discharge ($Q_{GM}$), and baseflow ($Q_{BF}$). The snow and glacier melt in SPHY are calculated using a degree-day model [29] The details of the model setup, downscaling method, and calibration/validation using observed stations are given in [21]. The SPHY model domain covers the entire basin of the Karnali, with the outlet defined at Chisapani, where the river transitions from the Siwalik Hills to the Terai.

## Future climate forcing

We used the Inter-Sectoral Impact Model Intercomparison Project Phase 3b (ISIMIP3b) global climate models (GCMs) output as climate change scenarios. ISIMIP3b is based on the Coupled Model Intercomparison Project Phase 6 (CMIP6) climate change scenarios for different global warming levels, combined with socio-economic scenarios [30]. The ISIMIP3b data is available for the following five CIMIP6 GCMs: GFDL-ESM4, IPSL-CM6A-LR, MPI-ESM1-2-HR, MRI-ESM2-0, and UKESM1-0-LL. In this study, we utilize these five GCMs for the three emission scenarios SSP1-2.6, SSP3-7.0, and SSP5-8.5. To ensure temporal and spatial consistency between the

This manuscript is a preprint and has not been peer reviewed. The copyright holder has made the manuscript available under a Creative Commons Attribution 4.0 International (CC BY) license and consented to have it forwarded to EarthArXiv for public posting.

reference and future model runs, the precipitation and temperature data of the GCMs were downscaled to the model grid resolution using a monthly delta change approach [31]. The future forcing was available from 2015 to 2100 for $500 \times 500$ m spatial resolution at daily time steps for each climate model and each of the three emission scenarios. With five climate models and three emission scenarios, we have 15 different climate forcings for the future climate runs. These future projections were then used in the previously calibrated model to simulate future scenarios until 2100.

## Analysis of future climate changes

First, the projected changes in precipitation and temperature were evaluated. The climatic variables were computed for two 30-year time windows: mid century (2041-2070) and late century (2071-2100). For precipitation, we computed the long-term mean of annual precipitation (P), both the $95^{\text{th}}$ (P95) and $99^{\text{th}}$ (P99) percentiles of daily precipitation, and the absolute maximum 5-day precipitation amount (RX5day). Similarly, we computed the long-term mean of annual minimum temperature ($\text{T}_{\text{min}}$), maximum temperature ($\text{T}_{\text{max}}$), and mean temperature ($\text{T}_{\text{mean}}$). The climatic variables were then compared against the values for the reference period (1991-2020) to quantify the projected changes. This comparison was performed separately for each future time slice (mid and late century), for each emissions scenario, and for each climate model.

Next, to assess projected changes in seasonal precipitation, we examined the distribution of the ensemble mean precipitation series using decadal box plots for each season and for each scenario. The standard deviation (SD) of seasonal precipitation within each decade was also calculated. We used these statistics to evaluate changes in both the magnitude and the variability of precipitation relative to the historical reference period.

In addition, we applied the Mann-Kendall test (MK-test) in two ways. First, an MK-test was conducted of the full transient annual precipitation series spanning from the reference period to the end of the century to detect long-term trends. Secondly, an MK-test was applied to the seasonal precipitation series where analysis was performed independently for the reference (historical), mid-century, and late-century periods. A precipitation series was considered to be statistically significant when the p-value$<$0.05.

Furthermore, we investigated the elevation dependence of the precipitation phase. As the Karnali basin covers a wide elevation range from the Tibetan Plateau to the Terai, the phase of precipitation is highly variable. With future warming, the precipitation phase is subject to change, and likely to have a large hydrological impact. To examine how the precipitation phase will change at different elevations under future climatic conditions, we stratified the basin into discrete elevation bands of 1000 m using a digital elevation model (DEM). For each band, we aggregated seasonal rainfall and snowfall and computed their fractions relative to the total precipitation. In SPHY, the phase of precipitation is based on the temperature threshold provided during calibration, which is $+2\,^{\circ}$C for the Karnali basin. We then computed the snowfall fraction (SF) as:

$$\text{SF}(z) = \frac{P_{\text{snow}}(z)}{P(z)}, \tag{1}$$

$$\Delta\text{SF}(z) = \text{SF}_{\text{fut}}(z) - \text{SF}_{\text{ref}}(z), \tag{2}$$

where $P(z)$ is the total seasonal precipitation in the elevation band $z$ and $P_{\text{snow}}(z)$ is the corresponding seasonal snowfall total. $\text{SF}(z)$ denotes the snowfall fraction, and $\Delta\text{SF}(z)$ is the change in snowfall fraction between the reference period (ref) and a given future window (fut). Snowfall fractions were computed for each climate model and emissions scenario, and changes were evaluated by differencing the reference period against each future period.

This manuscript is a preprint and has not been peer reviewed. The copyright holder has made the manuscript available under a Creative Commons Attribution 4.0 International (CC BY) license and consented to have it forwarded to EarthArXiv for public posting.

### Analysis of future hydrological changes

We quantified projected changes in river discharge at the basin outlet by comparing a reference period (1991–2020) with two future 30-year windows: mid century (2041–2070) and late century (2071–2100), under SSP1-2.6, SSP3-7.0, and SSP5-8.5. For total discharge, we computed the long-term mean annual discharge for the reference period and each future window and expressed projected changes as percentage differences relative to the reference. To analyze the temporal changes, we calculated long-term mean daily hydrograph for the reference and future periods. Future periods hydrograph are derived from the multi-model ensemble mean, with inter-model variability represented by ±1 SD. For the potential shifts in the timing of flow contributions, we calculated the cumulative fraction of annual discharge for each day of the year and computed the difference between future and reference cumulative fractions (Δ CF), where positive values indicate that a larger fraction of annual discharge is accumulated earlier in the year and negative values indicate delayed accumulation.

The difference in CF of annual discharge per day (d) was computed from the long-term mean daily discharge series as:

$$Q_{\text{ann}} = \sum_{d=1}^{365} Q(d) \tag{3}$$

$$\text{CF}(d) = \frac{\sum_{i=1}^{d} Q(i)}{\sum_{i=1}^{365} Q(i)} \tag{4}$$

$$\Delta\text{CF}(d) = \text{CF}_{\text{fut}}(d) - \text{CF}_{\text{ref}}(d) \tag{5}$$

Note that the value of CF is normalized to unity at the end of the year, which is $\text{CF}(365) = 1$ for both periods and therefore $\Delta\text{CF}(365) = 0$ by definition. The difference $\Delta\text{CF}(d)$ represents a redistribution of the annual discharge timing and should be interpreted as relative timing metric rather than changes in absolute discharge volume.

### Changes in water yield zones

For each runoff component (rainfall runoff, snowmelt and baseflow), total runoff, and actual evapotranspiration, we calculated long-term mean annual values for the reference period and for near-, mid-, and late-century projections under each SSP and climate model for each 1000 m elevation zone in $\text{km}^3\ \text{yr}^{-1}$. We quantified climate change impacts as absolute (Δ) differences between future periods and the reference, both for individual climate models and for the multi-model ensemble. We also summarized these changes as elevation dependent water yield zones. Although the contribution from the glacier melt is simulated in the model, it is not discussed in the result section as the contribution to the total discharge is very small compared with other runoff components.

## Results and discussion

### Precipitation and temperature

Both annual precipitation and temperature will increase by the end of the $21^{\text{st}}$ century under all scenarios, suggesting warmer and wetter future conditions ( S1 Fig and S2 Fig). The projected changes in precipitation and temperature for the mid- and late-century periods are given in S1 Table. By the end of the century, average annual precipitation for the ensemble of models is projected to increase within a range of $19 - 38\,\%$ across SSP1-2.6 to SSP5-8.5. In the mid-century period, SSP5-8.5 exhibits a

This manuscript is a preprint and has not been peer reviewed. The copyright holder has made the manuscript available under a Creative Commons Attribution 4.0 International (CC BY) license and consented to have it forwarded to EarthArXiv for public posting.

significant increasing trend, with a Sen's slope of $15.2\,\mathrm{mm\,yr^{-1}}$. In the late-century period, significant increasing trends are projected under both SSP3-7.0 and SSP5-8.5, with slopes of $10.7\,\mathrm{mm\,yr^{-1}}$ and $20.8\,\mathrm{mm\,yr^{-1}}$, respectively. Similarly, the ensemble mean annual temperature is projected to increase by $1.5-5.1\,^{\circ}\mathrm{C}$ by the end of the century for SSP1-2.6 to SSP5-8.5 respectively.

Although the projected annual precipitation shows a general increasing trend for the future, the seasonal trends are diverse. Fig 2 shows the seasonal precipitation distribution for each decade in the reference period and future periods based on the ensemble mean of models for different scenarios. In both the mid- and late-century periods, monsoon precipitation shows noticeable shifts compared to the reference period under all scenarios (Fig 2A). The decadal mean and median, along with the lower (Q1) and upper quartiles (Q3), generally show an upward shift in the future distribution relative to the reference period. The concurrent increase in SD suggests that monsoonal precipitation becomes more variable in the future. During the mid-century period, a statistically significant increase is projected under SSP5-8.5, with monsoon precipitation increasing by $11.2\,\mathrm{mm\,yr^{-1}}$. By the late-century period, significant increasing trends are projected under both SSP3-7.0 and SSP5-8.5, with increases of $7.5\,\mathrm{mm\,yr^{-1}}$ and $16.7\,\mathrm{mm\,yr^{-1}}$, respectively.

For the post-monsoon season (Fig 2B), the mean precipitation is generally higher across all scenarios and decades. For the SSP5–8.5 scenario, Q1 decreases the most while Q3 increases across all scenarios relative to the reference period. In general, a larger interquartile range (IQR) and SD indicate an increasing variability in post-monsoon precipitation. For the winter season (Fig 2C), the decadal mean generally declines relative to the long-term reference seasonal mean, particularly for the SSP3–7.0 and SSP5–8.5 scenarios. The IQR narrows as Q1 increases and Q3 decreases. These changes suggest a reduced winter precipitation and its variability in the future.

For the pre-monsoon season (Fig 2D), precipitation is generally higher in the future relative to the reference period. In some decades, for example 2071–2080, SSP3–7.0 exhibits a stronger shift in the precipitation distribution than SSP5–8.5, with a higher median and larger IQR. This difference can most likely be attributed to internal climate variability rather than a systematic difference between scenarios, as a small number of anomalously wet years can influence the distribution. However, at the annual scale SSP5–8.5 shows a stronger increase in precipitation than SSP3–7.0 (see S1 Fig). Among the seasons, only monsoon precipitation exhibits a statistically significant increasing trend across future decades, while pre-monsoon, winter, and post-monsoon precipitation show no statistically significant trends despite notable changes in their distributional characteristics.

**Fig 2. Seasonal precipitation distribution for each decade in the reference period and for the future climate scenarios.** Box plots show the distribution of seasonal precipitation for the reference period (1991–2022) and future projections based on the ensemble mean for SSP1–2.6, SSP3–7.0, and SSP5–8.5.

Overall, these results indicate consistent warming across the Karnali basin throughout the 21st century. In contrast, project precipitation changes are seasonally variable but with an overallincrease in annual totals. These results are consistent with previous studies for the Karnali basin [14–16] and across HMA [5, 6, 12], which also reported continued warming and overall increase of precipitation. These studies also reveal that precipitation projections are uncertain and vary with climate model, season, and elevation.

Precipitation in the Karnali basin is elevation dependent and under the future warming climate, there will be a shift in the phase of precipitation from snowfall to rainfall across elevation bands. This shift in phase affects the timing and magnitude of

This manuscript is a preprint and has not been peer reviewed. The copyright holder has made the manuscript available under a Creative Commons Attribution 4.0 International (CC BY) license and consented to have it forwarded to EarthArXiv for public posting.

runoff contributions from rain and snowmelt along the different elevation bands. In fig 3, we show projected changes in the snowfall fraction ($\Delta$SF) across elevation bands for each season compared to the reference period for all climate scenarios. We focus here on the results of scenario SSP3-7.0, which is less extreme and considered a more plausible trajectory for the future than scenario SSP5-8.5 which is increasingly viewed as upper end scenario [32]. Seasonal changes in SF are shown for each climate model compared to reference period across the mid- and late-century. A decline in the SF is evident across all elevation bands, indicated by negative $\Delta$SF values. This suggests a widespread shift in the precipitation phase from snow to rain.

During the winter season (DJF), the elevations between 2–4 km show the largest reduction in SF, with relatively small variability across climate models in both centuries, suggesting low inter-model uncertainty. By the late-century, $\Delta$SF is projected to reach a maximum decrease of $-0.59$ (model ipsl-cm6a-lr) in the elevation band of 3–4 km. In contrast at elevations above 5 km, $\Delta$SF values showed little to no change due to the low winter temperatures. During the pre-monsoon season (MAM), the decline in SF is evident at higher elevations ($> 4$ km). The magnitude of SF reduction is again more pronounced by the end of century, with considerable variability across climate models. In the elevation band of 4–5 km, $\Delta$SF in the late-century ranges from $-0.20$ to $-0.53$ across the climate models. A similar spread in $\Delta$SF between models is observed in other high elevation bands. During the monsoon season (JJAS), $\Delta$SF is projected negligible across all elevation bands as the monsoon precipitation is predominantly rainfall regardless of the warming climate. During the post-monsoon season (ON), the largest $\Delta$SF decline is again observed at elevations $> 4$ km, with considerable inter-model variability, ranging from $-0.23$ to $-0.59$ in the 4–5 km elevation band, for example.

**Fig 3. Projected future changes in snowfall fraction of total precipitation.** Change in snowfall fraction compared to the reference period for the scenario SSP3-RCP7.0 across elevation bands in the basin for different seasons.

Overall, these results indicate a shift toward more rainfall dominated conditions, with important implication for snow storage, runoff timing and lower buffering capacity of the basin for both mid- and late-century in the future. The strongest snow to rain transition is projected during winter between 2–4 km elevation zone, where snowfall declines by up to $-0.59$ equivalent to snowfall decrease of 106 mm season$^{-1}$. This elevation zone covers 36% of the basin area including much of Middle and High Mountains and is highly sensitive to future warming. At higher elevation band between 4–5 km in the High Himalaya phase shift signals is more pronounced outside winter. The 4–5 km elevation band, which covers 26% of the basin area, the largest elevation band by area shows a clear decline in SF occurs in the pre- and post-monsoon seasons. As November precipitation marks the onset of snowfall in the upper basin, a decline in post-monsoon SF suggests a delayed start of seasonal snow accumulation. Although absolute snowfall loss in this band is relatively small with lowest of 5 mm season$^{-1}$, the snowfall fraction declines by about $-0.29$. This shows that even a small reduction in snowfall amount can indicate important shift in precipitation phase. Similar snow to rain transitions have also been reported in other mountainous region for example, [33] used observations and climate model projections in the Peruvian Andes to estimate future shifts in precipitation phase and also showed a reduction in solid precipitation in the future.

In this study, we use climate projections and a temperature threshold approach to estimate future changes in precipitation phase. In reality, the actual processes controlling phase partitioning are more complex and influenced by the humidity and atmospheric conditions. These controls are important in the Karnali basin, where strong elevation gradients and complex terrain shape local meteorological conditions.

This manuscript is a preprint and has not been peer reviewed. The copyright holder has made the manuscript available under a Creative Commons Attribution 4.0 International (CC BY) license and consented to have it forwarded to EarthArXiv for public posting.

An earlier study by Dai et al. [34] reports that snow rain transition does not occur at a fixed temperature threshold, but occurs over a wider temperature range of a few degrees and also varies with atmospheric pressure. Our result show that the strongest decline in snowfall fraction between 2–4 km elevation range. Since we only use a temperature threshold to partition between rain and snow some uncertainty is introduced. However reliable estimates of relative humidity are not available. Limited change is projected above 4 km during winter because these elevations remain sufficiently cold for precipitation to fall predominantly as snow, even under future warming and this is consistent with Ding et al. [35]. A more robust assessment of future phase shifts would require meteorological observations and phase discrimination methods such as using energy balance or incorporating humidity as highlighted in studies by [36,37]. Such observations are limited in the Karnali basin. Despite these uncertainties, the analysis provides useful insights into the magnitude and elevation dependent distribution of $\Delta$SF and its implications for future hydrological change in the Karnali basin.

## Change in hydrology

### Total discharge and its components

Projected changes in future precipitation and temperature will impact the timing and magnitude of river discharge. Across all scenarios, the long-term mean annual discharge at the outlet of the Karnali basin increases for both mid and late century relative to the reference period. Fig 4A presents the long-term mean annual discharge of 1298 $m^3\,s^{-1}$ for the reference period (1991–2020) and the corresponding projected changes at the basin outlet under future scenarios. By mid century, the discharge increases by 29%, 30%, and 35% under SSP1–2.6, SSP3–7.0, and SSP5–8.5, respectively. By late century, the change becomes more pronounced, with increments of 35%, 45%, and 59% under SSP1–2.6, SSP3–7.0, and SSP5–8.5, respectively. The increase is more pronounced for the high emission scenarios. Projected changes are larger for high-flow than low-flow conditions, with ensemble Q10 increasing by 26–36% in the mid-century and 34–59% in the late-century, compared with Q90 increases of 9–13% and 17–34%, respectively. The corresponding flow duration curves are shown in S4 Fig, and the underlying values for the discharge are provided in S1 Table. Although Q10 represents frequently exceeded high-flow conditions rather than extreme flood return levels, the projected increase is in line with flood frequency projections for the Karnali basin which report a 79% increase in the 1% annual exceedance probability flood by the end of the century under a high-emission scenario [18].

**Fig 4. Reference discharge and projected changes for future climate scenarios for the late-century period at Chisapani outlet.** (A) Long-term mean annual discharge value ($m^3\,s^{-1}$) for the reference period and the projected relative change in annual discharge for the mid-century (2041-2070) and late-century (2071-2100) period at the basin outlet. The colored band represents the ensemble mean ± SD% across the climate models. (B) Comparison of the long-term mean future hydrograph components and total discharge during the reference period and the late-century period. The solid lines show the ensemble mean for each SSPs and colored band represents the ensemble mean ± SD across the climate models. (C) Heat map showing the difference in cumulative discharge fraction between the reference period and late-century projections as a function of day of year. Positive values (blue) indicate a larger fraction of annual discharge is generated earlier in the year and the negative values (brown) indicate a delayed runoff generation.

In addition to changes in total discharge magnitude, our results indicate a clear shift in the timing of water availability. Fig 4B compares the long-term mean daily hydrograph of the discharge components in the late-century period for the future scenarios relative to the reference period. The mid-century hydrograph is shown in supplementary S3 Fig which shows similar but less strong changes. For all future

This manuscript is a preprint and has not been peer reviewed. The copyright holder has made the manuscript available under a Creative Commons Attribution 4.0 International (CC BY) license and consented to have it forwarded to EarthArXiv for public posting.

scenarios, rainfall runoff ($Q_{\mathrm{RR}}$), baseflow ($Q_{\mathrm{BF}}$), and total discharge ($Q_{\mathrm{Tot}}$) are increasing. The snowmelt discharge ($Q_{\mathrm{SM}}$) is declining, with the strongest reduction towards the end of the century for SSP5–8.5 as a result of the precipitation phase shift. A pronounced shift in timing for $Q_{\mathrm{SM}}$ is also observed in the $\Delta$CF heat map (Fig 4C), where positive values indicate earlier snow accumulation relative to the reference period. The reduction in contribution from $Q_{\mathrm{SM}}$ is consistent with a projected decline in SF. During the reference period, $Q_{\mathrm{SM}}$ at the outlet peaks on day 179 (28 June), but shifts by 5, 14, and 43 days earlier for scenarios SSP1–2.6, SSP3–7.0, and SSP5–8.5, respectively. During the reference period, 50% of annual snowmelt discharge is generated by day 175 (24 June), but is 4, 23, and 33 days earlier for the SSP1–2.6, SSP3–7.0, and SSP5–8.5 scenarios, respectively. The change in the timing of $Q_{\mathrm{Tot}}$ at the outlet is relatively small. By the late-century, the peak $Q_{\mathrm{Tot}}$ occurs only 11-12 days earlier, while the timing of 50% of annual total discharge advances by only 2-7 days across scenarios. This relatively small shift in $Q_{\mathrm{Tot}}$ results from the compensation of a decrease in snowmelt by an increase in rainfall runoff and baseflow, a pattern consistent with the findings for the Ganges basin [8]. Pink et al. [18] also reported that warming shifts meltwater generation earlier in the season, thereby lowering the snowmelt contribution to large flood events in monsoon. Across the wider HMA, Kraaijenbrink et al. [7] also project a continued decline in the contribution of snowmelt to runoff under future warming.

Although the hydrograph indicates clear changes in flow magnitude and timing, the overall seasonal partitioning of annual discharge at the downstream outlet shows only a limited redistribution. In the reference period, the monsoon period discharge accounts for 71% of annual discharge which declines by 2.4%, 3.1% and 4.0% under SSP1–2.6, SSP3–7.0, and SSP5–8.5, respectively by end of century. In contrast, the post-monsoon share increases by 1.7%, 2.0% and 3.1% under same scenarios. Winter contributions changes only marginally, by +0.1%, −0.8% and −0.5% under SSP1–2.6, SSP3–7.0, and SSP5–8.5, respectively. These results highlight that future change in discharge occur mostly within the different seasons defined.

Overall, the results show that the future climate will shape the discharge regime of Karnali basin altering both magnitude and temporal distribution with high variability. Even if changes in seasonal totals are small, shifts in timing at the sub-seasonal scale have important implications for water availability that are not evident from seasonal totals alone. Therefore, these results provide an important reference to interpreting change in future hydrology across multiple temporal scales. However, the projected discharge changes are reported as multi-model ensemble means, but the spread between simulated discharge from climate models reflect the uncertainty (Fig 4B). Direct comparison of projected discharge with previous climate change studies in Karnali is complicated because studies differ in climate forcing, bias correction, reference period, and hydrological model structure. Despite these differences, the direction of change is similar. The previous studies also project warming, reduced snowmelt contribution, and increased precipitation, especially during the monsoon, leading to increased discharge in the Karnali basin [14, 15, 18]. The magnitude of change projected here should therefore be interpreted in the context of the selected climate model ensemble. For this study, ISIMIP3b seems suitable as it is taken from CMIP6 based forcing and that has already been bias adjusted and statistically downscaled using a trend preserving quantile mapping approach developed for climate change impact studies. Its bias adjustment is based on W5E5 which is bias adjusted ERA5 making it consistent with the ERA5 based historical forcing that we use in our study [28, 30, 38, 39] .

### Water yield zones

We analyzed changes in annual water fluxes relative to the reference period across elevation bands for each climate model for all climate change scenarios. Fig 5 shows

This manuscript is a preprint and has not been peer reviewed. The copyright holder has made the manuscript available under a Creative Commons Attribution 4.0 International (CC BY) license and consented to have it forwarded to EarthArXiv for public posting.

absolute changes ($\Delta$) in $ET_A$, $Q_{SM}$, $Q_{RR}$ and $Q_{Tot}$ for scenario SSP3–7.0. The results for scenarios SSP1–2.6 and SSP5–8.5 are given in S5 Fig. Across both future periods, the elevation bands exhibiting the strongest change remain similar, but the magnitude of change is more pronounced for the late century, which is therefore a focus here.

The spatial pattern of change in water fluxes exhibits a clear relation with elevation. $ET_a$ varies and shows both increases and decreases along the elevation. $ET_a$ increases mainly in the higher-elevation zones ($> 3$ km), with the largest increase in the 4–5 km elevation zone ($+1.8$ km$^3$ yr$^{-1}$), indicating enhanced evaporative losses under warmer future conditions where moisture remains available. In contrast, $ET_a$ decreases at lower elevations, with the strongest decrease in the 1–2$\tilde{\text{km}}$ elevation band($-1.0$ km$^3$yr$^{-1}$), despite increasing temperature along these elevation. Rainfall runoff $Q_{RR}$ increases across all elevation bands, with the largest increase occurring in the 1–2 km elevation band($+7.4$ km$^3$yr$^{-1}$). The increase in $Q_{RR}$ along the elevation zones is driven by higher precipitation and phase shift of precipitation from snowfall towards rainfall. Snowmelt contribution $Q_{SM}$ declines over all elevation band and the strongest decrease is observed between 3–5 km ($-0.7$ km$^3$yr$^{-1}$) driven by transition of precipitation from snow to rain due to warming. Baseflow $Q_{BF}$ increases along the elevation band with the largest increase projected to occur between 3–4 km ($+3.0$ km$^3$yr$^{-1}$), likely due to increased infiltration from additional rainfall.

**Fig 5. Elevation dependent changes in water yield zones.** Absolute change in long-term mean annual water fluxes ($\Delta$, km$^3$,yr$^{-1}$) for SSP3–7.0 scenario relative to the reference period (1991–2020) across elevation bands for rainfall runoff ($Q_{RR}$), snowmelt discharge ($Q_{SM}$), baseflow ($Q_{BF}$), total discharge ($Q_{Tot}$), and actual evapotranspiration (ETa). Thin dashed lines represent individual climate model, while thick lines show the multi-model mean for mid-century (2041–2070) and late-century (2071–2100), respectively. Positive values indicate increases relative to the reference period and negative values indicate decreases.

The result suggest that future changes in total runoff are not uniform across Karnali basin but are controlled by individual water balance components. The decrease in $ET_a$ at lower elevations $< 3$ km, despite increasing temperature and monsoon precipitation, suggests that future changes in evapotranspiration are not controlled by water input alone. Actual evapotranspiration in the basin is controlled by atmospheric demand, radiation, humidity, vegetation properties and the seasonal timing of precipitation [40]. These elevation band receives increased monsoon precipitation, but when humidity and cloud cover are high and evaporative demand can be relatively low. Under such condition, precipitation can turn into direct rain runoff and baseflow than contributing for $ET_a$. To support this interpretation, we performed additional diagnostic checks on wet day (basin average $P > 1$ mm d$^{-1}$) frequency (see S6 Fig). These checks indicate that future precipitation becomes concentrated into fewer, heavier rainfall events, causing root zone runoff to increases and root water storage to decreases. The lower elevation (1–2 km), covering the Siwalik, and parts of the Middle Mountains become more important for rainfall runoff generation. At higher elevation (3–5 km), spanning the Middle Mountains and partly the High Himalaya, warming increases $ET_a$ and reduces $Q_{SM}$ in the present snow rain transition zone which can be called the climate sensitive zone for the Karnali basin. This contrasting responses along the basin indicate redistribution of water fluxes across elevation bands where increase in $Q_{RR}$ and $Q_{BF}$ compensates the decline in contribution from $Q_{SM}$ and contribute to the higher total discharge. Such a shift may increase annual water availability at the outlet, but it can also increase the sensitivity of downstream flows to monsoon precipitation variability and high intensity rainfall events.

This manuscript is a preprint and has not been peer reviewed. The copyright holder has made the manuscript available under a Creative Commons Attribution 4.0 International (CC BY) license and consented to have it forwarded to EarthArXiv for public posting.

# Conclusion

In this study, we analyzed the future changes in climate and hydrology of the Karnali river basin under climate change. Both precipitation (P) and total average discharge ($Q_{Tot}$) are projected to increase towards the end of the 21$^{st}$ century. The magnitude of the projected increase varies between the climate models. By late century, the change in $Q_{Tot}$ becomes more pronounced, with increments of 35.2%, 45.2%, and 58.6% under SSP1–2.6, SSP3–7.0, and SSP5–8.5, respectively. However, our results show that the future hydrological change in the Karnali basin is driven by a change in timing and magnitude across temporal scales and elevation dependent shifts in water balance components. For the future emission scenarios, P increasingly falls as rain reducing the seasonal snow storage. As a result, snowmelt runoff ($Q_{SM}$) shifts earlier in the year, with the peak occurring 33 days earlier under SSP5–8.5 by the late-century, and its contribution progressively declines towards the end of the century. At the same time, contribution from surface runoff ($Q_{RR}$) and baseflow ($Q_{BF}$) becomes more important.

A key finding of this study is that future hydrological change in the Karnali basin is strongly elevation dependent. In the lower-elevation zones, especially around 1–2 km, increasing precipitation and a shift from snowfall to rainfall enhance rainfall runoff ($Q_{RR}$) and baseflow ($Q_{BF}$), while $ET_a$ decreases. In the mid- to high-elevation transition zone between 3–5 km, warming reduces snow storage and snowmelt runoff ($Q_{SM}$), while $ET_a$ increases. Above 5 km, absolute changes are smaller. These elevation dependent changes show that the future increase in total discharge ($Q_{Tot}$) is not caused by a uniform increase across the basin, but by a redistribution of water balance components such as increasing $Q_{RR}$ and $Q_{BF}$ compensate for declining $Q_{SM}$.

Seasonally, the basin shifts towards a more rainfall dominated regime. Snowmelt occurs earlier and contributes less towards the end of the century, while monsoon rainfall runoff and baseflow become more important for sustaining total discharge. As a result, $Q_{Tot}$ increases under all future scenarios, but the buffering role of seasonal snow storage weakens. This implies that future discharge at Chisapani may become more sensitive to monsoon precipitation variability and high intensity rainfall events.

These changes have important downstream implications. A more rainfall driven and less buffered basin is likely to be more sensitive to precipitation variability, with increased flood risk, droughts during low flow periods, and shifts in seasonal water availability that may affect irrigation, hydropower, ecosystems, and infrastructure at different elevations of the basin. These findings underline that future hydrological changes in mountainous basins like Karnali are best understood not as change in totals at the outlet, but as an elevation dependent redistribution of hydrological components. Future studies should therefore explore elevation dependent changes, because basin average responses can mask the zones where climate sensitivity is greatest and where changes in water balance components are most likely to reshape downstream discharge.

This manuscript is a preprint and has not been peer reviewed. The copyright holder has made the manuscript available under a Creative Commons Attribution 4.0 International (CC BY) license and consented to have it forwarded to EarthArXiv for public posting.

# Supporting information

**S1 Fig. Line plot of historical and future annual precipitation distributions.** The different colored lines show annual precipitation values for the reference period (1991–2022) and future projections based on the ensemble mean of climate models under SSP1-2.6, SSP3-7.0, and SSP5-8.5.

**S2 Fig. Line plot of historical and future annual mean temperature ($T_{avg}$) distributions.** The different colored lines show annual $T_{avg}$ values for the reference period (1991–2022) and future projections based on the ensemble mean of climate models under SSP1-2.6, SSP3-7.0, and SSP5-8.5.

**S1 Table. Projected changes in precipitation extremes, precipitation, temperature, and discharge across scenarios and models.** Notes: P90/P95/P99 denote the 90th/95th/99th percentile of daily precipitation; Rx5day is the maximum 5-day precipitation total. Percent values denote change relative to the reference period value (1991–2020). Temperature values are absolute changes (°C). Q90 and Q10 are reported as absolute discharge values.

**S3 Fig. Reference discharge and projected changes under future climate scenarios for the mid-century period (2041-2070).** (A) Comparison of the long-term mean future hydrograph components and total discharge ($m^3\,s^{-1}$) during the reference period and the mid-century period (2041-2070). The solid lines show the ensemble mean for each SSPs, and colored band represents the ensemble mean ± SD across the climate models. (B) Heat map showing the difference in cumulative discharge fraction between the reference period and late-century projections as a function of day of year. The positive value indicates a larger fraction of annual discharge accumulated earlier in the year and negative value indicates delayed accumulation.

**S4 Fig. Flow duration curves of daily discharge for the reference period and future climate scenarios.** (A) Flow duration curves for the mid-century period (2041–2070) under each SSP scenario compared with the reference period (1991–2020). (B) Flow duration curves for the late-century period (2071–2100) under each SSP scenario compared with the reference period (1991–2020).

**S5 Fig. Elevation dependent changes in water yield zones under SSP1–2.6 and SSP5–8.5. ($T_{avg}$) distributions.** Absolute change in long-term mean annual water fluxes ($\Delta$, $km^3\,yr^{-1}$) relative to the reference period (1991–2020) across 1-km elevation bands for (Rain runoff, Snowmelt, Baseflow, Total discharge, and Actual ET). Panels show projections under SSP1-2.6 and SSP5-8.5. Thin dashed lines represent individual climate-model differences, while thick lines show the multi-model mean.Positive values indicate increases relative to the reference period and negative values indicate decreases.

**S6 Fig. Seasonal wet day frequency under reference and future climate conditions.** Wet days were defined as days with basin average precipitation $P > 1$ mm $d^{-1}$. Panels show the annual number of wet days for each season during the reference period (1991–2020), mid-century period (2041–2070), and late-century period (2071–2100) under SSP1–2.6, SSP3–7.0, and SSP5–8.5. This diagnostic analysis supports the interpretation that future precipitation becomes concentrated into fewer, heavier events, which can increase runoff generation while reducing sustained water availability for $ET_a$.

This manuscript is a preprint and has not been peer reviewed. The copyright holder has made the manuscript available under a Creative Commons Attribution 4.0 International (CC BY) license and consented to have it forwarded to EarthArXiv for public posting.

## Acknowledgments

The authors are also thankful to Future Water (Wageningen, the Netherlands) for providing the source code for the SPHY model in the public domain.

## References

1. Viviroli D, Kummu M, Meybeck M, Kallio M, Wada Y. Increasing dependence of lowland populations on mountain water resources. Nature Sustainability. 2020 Nov;3(11):917-28. Publisher: Nature Publishing Group. Available from: https://www.nature.com/articles/s41893-020-0559-9. doi:10.1038/s41893-020-0559-9.

2. Immerzeel WW, van Beek LPH, Bierkens MFP. Climate Change Will Affect the Asian Water Towers. Science. 2010 Jun;328(5984):1382-5. Publisher: American Association for the Advancement of Science. Available from: https://www.science.org/doi/full/10.1126/science.1183188. doi:10.1126/science.1183188.

3. Intergovernmental Panel on Climate Change (IPCC). Climate Change 2022 – Impacts, Adaptation and Vulnerability: Working Group II Contribution to the Sixth Assessment Report of the Intergovernmental Panel on Climate Change. 1st ed. Cambridge University Press; 2023. Available from: https://www.cambridge.org/core/product/identifier/9781009325844/type/book. doi:10.1017/9781009325844.

4. Gobiet A, Kotlarski S, Beniston M, Heinrich G, Rajczak J, Stoffel M. 21st century climate change in the European Alps—A review. Science of The Total Environment. 2014 Sep;493:1138-51. Available from: https://www.sciencedirect.com/science/article/pii/S0048969713008188. doi:10.1016/j.scitotenv.2013.07.050.

5. Lutz AF, Immerzeel WW, Kraaijenbrink PDA, Shrestha AB, Bierkens MFP. Climate Change Impacts on the Upper Indus Hydrology: Sources, Shifts and Extremes. PLOS ONE. 2016 Nov;11(11):e0165630. Publisher: Public Library of Science. Available from: https://journals.plos.org/plosone/article?id=10.1371/journal.pone.0165630. doi:10.1371/journal.pone.0165630.

6. Wijngaard RR, Lutz AF, Nepal S, Khanal S, Pradhananga S, Shrestha AB, et al. Future changes in hydro-climatic extremes in the Upper Indus, Ganges, and Brahmaputra River basins. PLOS ONE. 2017 Dec;12(12):e0190224. Publisher: Public Library of Science. Available from: https://journals.plos.org/plosone/article?id=10.1371/journal.pone.0190224. doi:10.1371/journal.pone.0190224.

7. Kraaijenbrink PDA, Stigter EE, Yao T, Immerzeel WW. Climate change decisive for Asia's snow meltwater supply. Nature Climate Change. 2021 Jul;11(7):591-7. Publisher: Nature Publishing Group. Available from: https://www.nature.com/articles/s41558-021-01074-x. doi:10.1038/s41558-021-01074-x.

8. Khanal S, Lutz AF, Kraaijenbrink PDA, Hurk Bvd, Yao T, Immerzeel WW. Variable 21st Century Climate Change Response for Rivers in High Mountain Asia at Seasonal to Decadal Time Scales. Water Resources Research. 2021 May;57(5):e2020WR029266. Publisher: John Wiley & Sons, Ltd. Available from:

This manuscript is a preprint and has not been peer reviewed. The copyright holder has made the manuscript available under a Creative Commons Attribution 4.0 International (CC BY) license and consented to have it forwarded to EarthArXiv for public posting.

https://agupubs.onlinelibrary.wiley.com/doi/10.1029/2020WR029266. doi:10.1029/2020WR029266.

9. Bernat M, Miles ES, Kneib M, Fujita K, Sasaki O, Shaw TE, et al. Precipitation phase drives seasonal and decadal snowline changes in high mountain Asia. Environmental Research Letters. 2025 May;20(6):064039. Publisher: IOP Publishing. Available from: https://doi.org/10.1088/1748-9326/adcf39. doi:10.1088/1748-9326/adcf39.

10. Musselman KN, Clark MP, Liu C, Ikeda K, Rasmussen R. Slower snowmelt in a warmer world. Nature Climate Change. 2017 Mar;7(3):214-9. Publisher: Nature Publishing Group. Available from: https://www.nature.com/articles/nclimate3225. doi:10.1038/nclimate3225.

11. Musselman KN, Lehner F, Ikeda K, Clark MP, Prein AF, Liu C, et al. Projected increases and shifts in rain-on-snow flood risk over western North America. Nature Climate Change. 2018 Sep;8(9):808-12. Publisher: Nature Publishing Group. Available from: https://www.nature.com/articles/s41558-018-0236-4. doi:10.1038/s41558-018-0236-4.

12. Lalande M, Ménégoz M, Krinner G, Naegeli K, Wunderle S. Climate change in the High Mountain Asia in CMIP6. Earth System Dynamics. 2021 Nov;12(4):1061-98. Publisher: Copernicus GmbH. Available from: https://esd.copernicus.org/articles/12/1061/2021/. doi:10.5194/esd-12-1061-2021.

13. Han J, Liu Z, Woods R, McVicar TR, Yang D, Wang T, et al. Streamflow seasonality in a snow-dwindling world. Nature. 2024 May;629(8014):1075-81. Publisher: Nature Publishing Group. Available from: https://www.nature.com/articles/s41586-024-07299-y. doi:10.1038/s41586-024-07299-y.

14. Pandey VP, Dhaubanjar S, Bharati L, Thapa BR. Spatio-temporal distribution of water availability in Karnali-Mohana Basin, Western Nepal: Climate change impact assessment (Part-B). Journal of Hydrology: Regional Studies. 2020 Jun;29:100691. Available from: https://www.sciencedirect.com/science/article/pii/S2214581820301658. doi:10.1016/j.ejrh.2020.100691.

15. Dhaubanjar S, Prasad Pandey V, Bharati L. Climate futures for Western Nepal based on regional climate models in the CORDEX-SA. International Journal of Climatology. 2020;40(4):2201-25. _eprint: https://rmets.onlinelibrary.wiley.com/doi/pdf/10.1002/joc.6327. Available from: https://onlinelibrary.wiley.com/doi/abs/10.1002/joc.6327. doi:10.1002/joc.6327.

16. Dahal P, Shrestha ML, Panthi J, Pradhananga D. Modeling the future impacts of climate change on water availability in the Karnali River Basin of Nepal Himalaya. Environmental Research. 2020 Jun;185:109430. Available from: https://www.sciencedirect.com/science/article/pii/S0013935120303236. doi:10.1016/j.envres.2020.109430.

17. Pradhananga S, Nepal S, Kamal SK, Hafeez M. Climate change will exacerbate seasonal flow variability in the Karnali River basin: Implications for water, energy, and agriculture sectors. Hydrology Research. 2025 May;56(6):471-91. Available from: https://doi.org/10.2166/nh.2025.193. doi:10.2166/nh.2025.193.

This manuscript is a preprint and has not been peer reviewed. The copyright holder has made the manuscript available under a Creative Commons Attribution 4.0 International (CC BY) license and consented to have it forwarded to EarthArXiv for public posting.

18. Pink I, Reaney SM, Hardy RJ, Bovolo CI. Increased rainfall-runoff drives flood hazard intensification in Central Himalayan river systems. Scientific Reports. 2025 Dec;15(1):42277. Publisher: Nature Publishing Group. Available from: https://www.nature.com/articles/s41598-025-26815-2. doi:10.1038/s41598-025-26815-2.

19. Adhikari BR, Ojha RB. Geology and Physiography. In: Ojha RB, Panday D, editors. The Soils of Nepal. Cham: Springer International Publishing; 2021. p. 29-39. Available from: https://doi.org/10.1007/978-3-030-80999-7_4. doi:10.1007/978-3-030-80999-$7_4$.

20. Sharma UC, Datta M, Sharma V. Physiography and Resources. In: Sharma UC, Datta M, Sharma V, editors. Soils in the Hindu Kush Himalayas: Management for Agricultural Land Use. Cham: Springer International Publishing; 2022. p. 59-93. Available from: https://doi.org/10.1007/978-3-031-11458-8_3. doi:10.1007/978-3-031-11458-$8_3$.

21. Pokhrel P, Griffioen J, Bogaard TA, Kraaijenbrink PDA, Fiddes J, Immerzeel WW. Upstream hydrology and the importance of snowmelt in buffering droughts in the Karnali basin in Nepal. Frontiers in Water. 2026;Volume 7 - 2025. Available from: https://www.frontiersin.org/journals/water/articles/10.3389/frwa.2025.1720178. doi:10.3389/frwa.2025.1720178.

22. Bookhagen B, Thiede RC, Strecker MR. Abnormal monsoon years and their control on erosion and sediment flux in the high, arid northwest Himalaya. Earth and Planetary Science Letters. 2005 Feb;231(1):131-46. Available from: https://www.sciencedirect.com/science/article/pii/S0012821X0400696X. doi:10.1016/j.epsl.2004.11.014.

23. Bookhagen B, Burbank DW. Topography, relief, and TRMM-derived rainfall variations along the Himalaya. Geophysical Research Letters. 2006;33(8). _eprint: https://agupubs.onlinelibrary.wiley.com/doi/pdf/10.1029/2006GL026037. Available from: https://onlinelibrary.wiley.com/doi/abs/10.1029/2006GL026037. doi:10.1029/2006GL026037.

24. Terink W, Lutz AF, Simons GWH, Immerzeel WW, Droogers P. SPHY v2.0: Spatial Processes in HYdrology. Geoscientific Model Development. 2015 Jul;8(7):2009-34. Publisher: Copernicus GmbH. Available from: https://gmd.copernicus.org/articles/8/2009/2015/. doi:10.5194/gmd-8-2009-2015.

25. Wijngaard RR, Biemans H, Lutz AF, Shrestha AB, Wester P, Immerzeel WW. Climate change vs. socio-economic development: understanding the future South Asian water gap. Hydrology and Earth System Sciences. 2018 Dec;22(12):6297-321. Publisher: Copernicus GmbH. Available from: https://hess.copernicus.org/articles/22/6297/2018/. doi:10.5194/hess-22-6297-2018.

26. Pradhan AMS, Silwal G, Shrestha S, Huynh TC, Dawadi S. Can a Spatially Distributed Hydrological Model Effectively Analyze Hydrological Processes in the Nepal Himalaya River Basin? Environmental Modeling & Assessment. 2024 Dec;29(6):1037-58. Available from: https://doi.org/10.1007/s10666-024-09975-9. doi:10.1007/s10666-024-09975-9.

This manuscript is a preprint and has not been peer reviewed. The copyright holder has made the manuscript available under a Creative Commons Attribution 4.0 International (CC BY) license and consented to have it forwarded to EarthArXiv for public posting.

27. Nepal J, Pant RR, Shrestha S, Paudel S, Bishwakarma K, Awasthi MP, et al. Water balance estimation and runoff simulation of Chameliya Watershed, Nepal. Environmental Earth Sciences. 2024 Jan;83(3):117. Available from: https://doi.org/10.1007/s12665-024-11430-7. doi:10.1007/s12665-024-11430-7.

28. Hersbach H, Bell B, Berrisford P, Hirahara S, Horányi A, Muñoz-Sabater J, et al. The ERA5 global reanalysis. Quarterly Journal of the Royal Meteorological Society. 2020;146(730):1999-2049. _eprint: https://rmets.onlinelibrary.wiley.com/doi/pdf/10.1002/qj.3803. Available from: https://onlinelibrary.wiley.com/doi/abs/10.1002/qj.3803. doi:10.1002/qj.3803.

29. Hock R. Temperature index melt modelling in mountain areas. Journal of Hydrology. 2003 Nov;282(1-4):104-15. Publisher: Elsevier BV. Available from: https://linkinghub.elsevier.com/retrieve/pii/S0022169403002579. doi:10.1016/s0022-1694(03)00257-9.

30. Lange S, Büchner M. ISIMIP3b bias-adjusted atmospheric climate input data. ISIMIP Repository; 2021. Version Number: 1.1. Available from: https://doi.org/10.48364/ISIMIP.842396.1. doi:10.48364/ISIMIP.842396.1.

31. Fowler HJ, Blenkinsop S, Tebaldi C. Linking climate change modelling to impacts studies: recent advances in downscaling techniques for hydrological modelling. International Journal of Climatology. 2007;27(12):1547-78. _eprint: https://rmets.onlinelibrary.wiley.com/doi/pdf/10.1002/joc.1556. Available from: https://onlinelibrary.wiley.com/doi/abs/10.1002/joc.1556. doi:10.1002/joc.1556.

32. Meinshausen M, Schleussner CF, Beyer K, Bodeker G, Boucher O, Canadell JG, et al. A perspective on the next generation of Earth system model scenarios: towards representative emission pathways (REPs). Geoscientific Model Development. 2024 Jun;17(11):4533-59. Publisher: Copernicus GmbH. Available from: https://gmd.copernicus.org/articles/17/4533/2024/. doi:10.5194/gmd-17-4533-2024.

33. Llactayo V, Valdivia J, Yarleque C, Callañaupa S, Villalobos-Puma E, Guizado D, et al. Future changes of precipitation types in the Peruvian Andes. Scientific Reports. 2024 Sep;14(1):22634. Publisher: Nature Publishing Group. Available from: https://www.nature.com/articles/s41598-024-71840-2. doi:10.1038/s41598-024-71840-2.

34. Dai A. Temperature and pressure dependence of the rain-snow phase transition over land and ocean. Geophysical Research Letters. 2008;35(12). _eprint: https://agupubs.onlinelibrary.wiley.com/doi/pdf/10.1029/2008GL033295. Available from: https://onlinelibrary.wiley.com/doi/abs/10.1029/2008GL033295. doi:10.1029/2008GL033295.

35. Ding B, Yang K, Qin J, Wang L, Chen Y, He X. The dependence of precipitation types on surface elevation and meteorological conditions and its parameterization. Journal of Hydrology. 2014 May;513:154-63. Available from: https://www.sciencedirect.com/science/article/pii/S0022169414002236. doi:10.1016/j.jhydrol.2014.03.038.

This manuscript is a preprint and has not been peer reviewed. The copyright holder has made the manuscript available under a Creative Commons Attribution 4.0 International (CC BY) license and consented to have it forwarded to EarthArXiv for public posting.

36. Harder P, Pomeroy J. Estimating precipitation phase using a psychrometric energy balance method. Hydrological Processes. 2013;27(13):1901-14. _eprint: https://onlinelibrary.wiley.com/doi/pdf/10.1002/hyp.9799. Available from: https://onlinelibrary.wiley.com/doi/abs/10.1002/hyp.9799. doi:10.1002/hyp.9799.

37. Sun F, Chen Y, Li Y, Li Z, Duan W, Zhang Q, et al. Incorporating relative humidity improves the accuracy of precipitation phase discrimination in High Mountain Asia. Atmospheric Research. 2022 Jun;271:106094. Available from: https://www.sciencedirect.com/science/article/pii/S0169809522000801. doi:10.1016/j.atmosres.2022.106094.

38. Lange S. Trend-preserving bias adjustment and statistical downscaling with ISIMIP3BASD (v1.0). Geoscientific Model Development. 2019 Jul;12(7):3055-70. Publisher: Copernicus GmbH. Available from: https://gmd.copernicus.org/articles/12/3055/2019/. doi:10.5194/gmd-12-3055-2019.

39. Cucchi M, Weedon GP, Amici A, Bellouin N, Lange S, Müller Schmied H, et al. WFDE5: bias-adjusted ERA5 reanalysis data for impact studies. Earth System Science Data. 2020 Sep;12(3):2097-120. Publisher: Copernicus GmbH. Available from: https://essd.copernicus.org/articles/12/2097/2020/. doi:10.5194/essd-12-2097-2020.

40. Collignan J, Polcher J, Bastin S, Quintana-Segui P. Budyko Framework Based Analysis of the Effect of Climate Change on Watershed Evaporation Efficiency and Its Impact on Discharge Over Europe. Water Resources Research. 2023 Oct;59(10):e2023WR034509. Publisher: John Wiley & Sons, Ltd. Available from: https://agupubs.onlinelibrary.wiley.com/doi/10.1029/2023WR034509. doi:10.1029/2023WR034509.

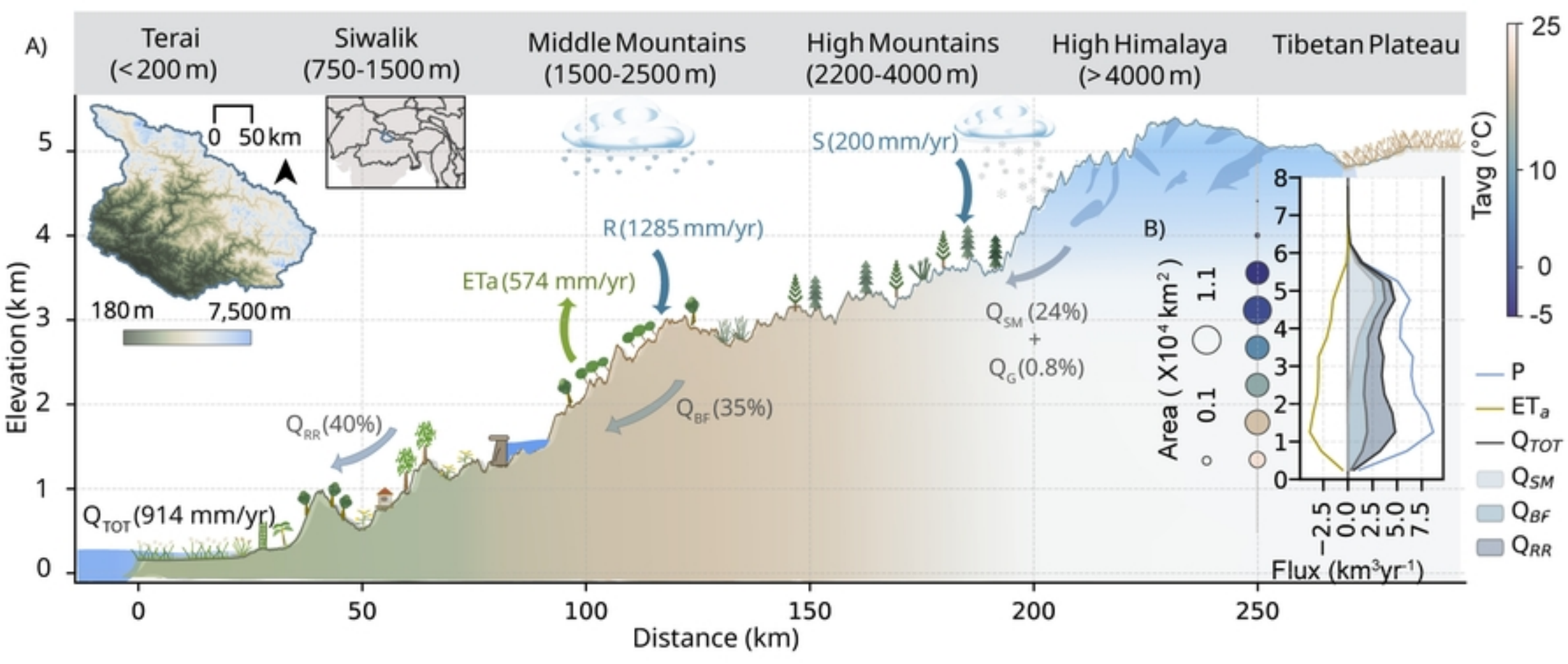
A)
Terai
(< 200 m)
Siwalik
(750-1500 m)
Middle Mountains
(1500-2500 m)
High Mountains
(2200-4000 m)
High Himalaya
(> 4000 m)
Tibetan Plateau
0 50 km
180 m
7,500 m
S (200 mm/yr)
R (1285 mm/yr)
ETa (574 mm/yr)
$Q_{SM}$ (24%)
+
$Q_G$ (0.8%)
$Q_{BF}$ (35%)
$Q_{RR}$ (40%)
$Q_{TOT}$ (914 mm/yr)
Elevation (km)
Distance (km)
B)
Area ( X10⁴ km²)
1.1
0.1
Flux (km³yr⁻¹)
Tavg (°C)
P
$ET_a$
$Q_{TOT}$
$Q_{SM}$
$Q_{BF}$
$Q_{RR}$

Fig 1

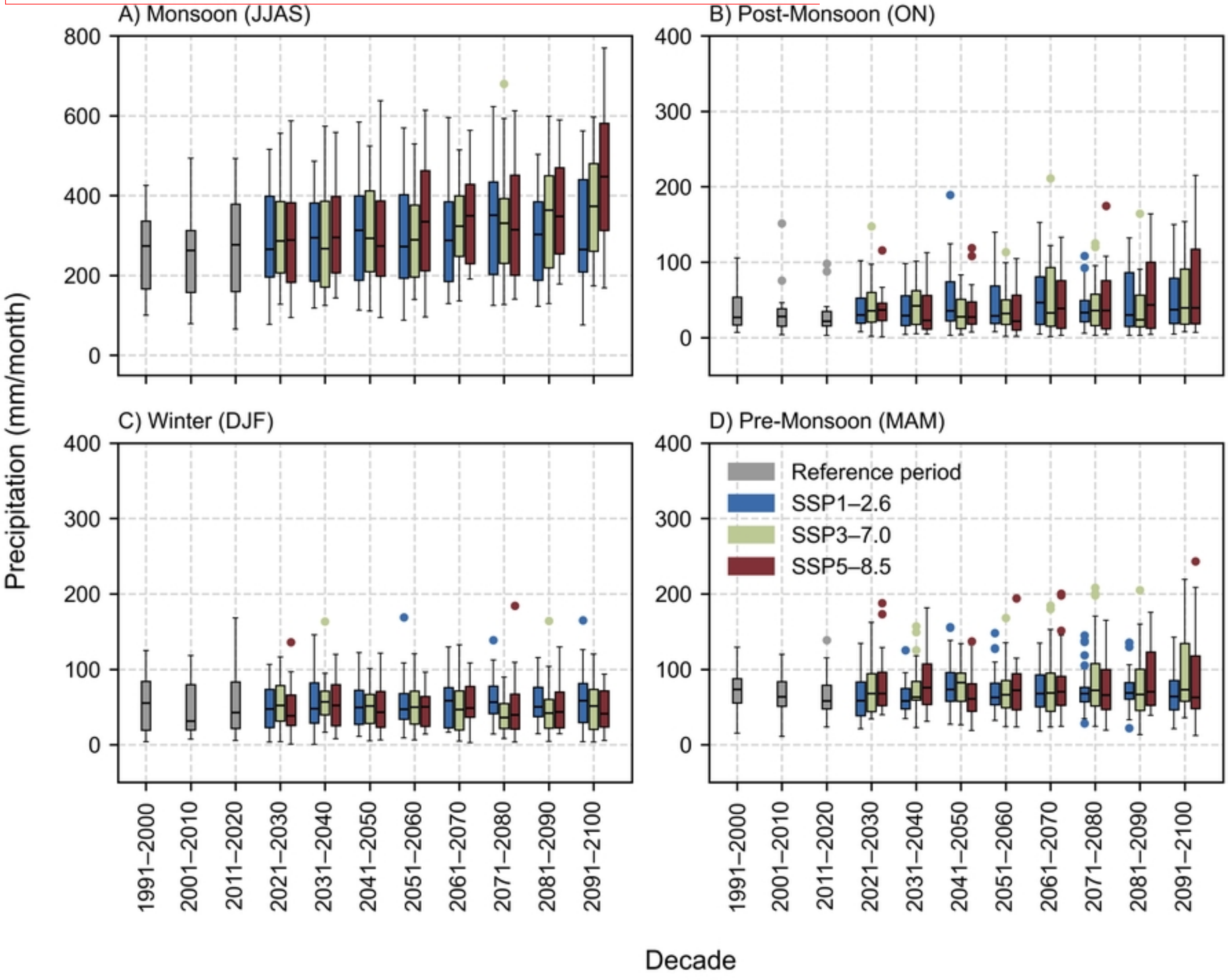
A) Monsoon (JJAS)
B) Post-Monsoon (ON)
C) Winter (DJF)
D) Pre-Monsoon (MAM)
Precipitation (mm/month)
Reference period
SSP1–2.6
SSP3–7.0
SSP5–8.5
1991–2000
2001–2010
2011–2020
2021–2030
2031–2040
2041–2050
2051–2060
2061–2070
2071–2080
2081–2090
2091–2100
Decade

Fig 2

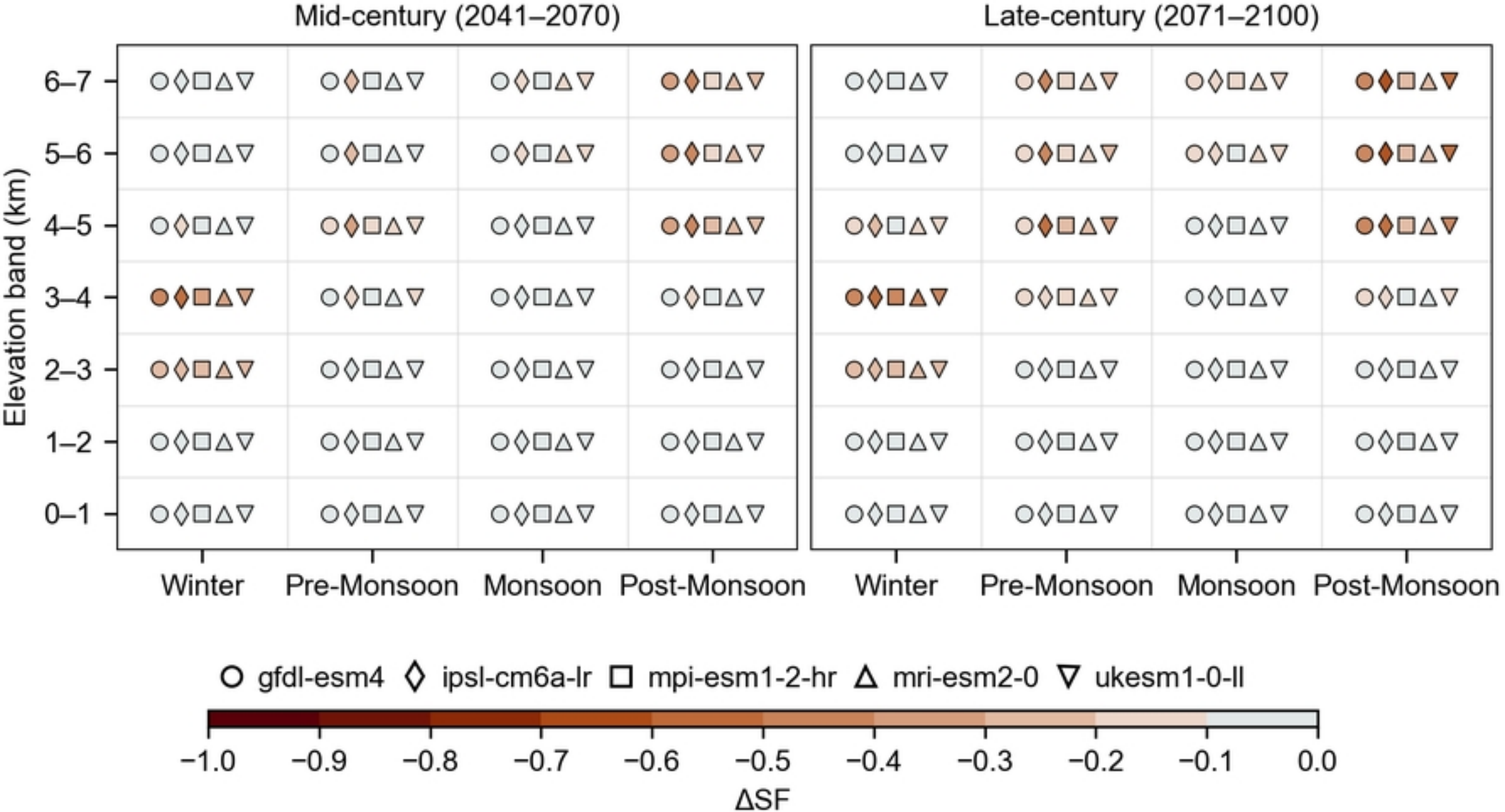
Mid-century (2041–2070)
Late-century (2071–2100)
Elevation band (km)
6–7
5–6
4–5
3–4
2–3
1–2
0–1
Winter
Pre-Monsoon
Monsoon
Post-Monsoon
gfdl-esm4
ipsl-cm6a-lr
mpi-esm1-2-hr
mri-esm2-0
ukesm1-0-ll
−1.0
−0.9
−0.8
−0.7
−0.6
−0.5
−0.4
−0.3
−0.2
−0.1
0.0
ΔSF

Fig 3

This manuscript is a preprint and has not been peer reviewed. The copyright holder has made the manuscript available under a Creative Commons Attribution 4.0 International (CC BY) license and consented to have it forwarded to EarthArXiv for public posting.

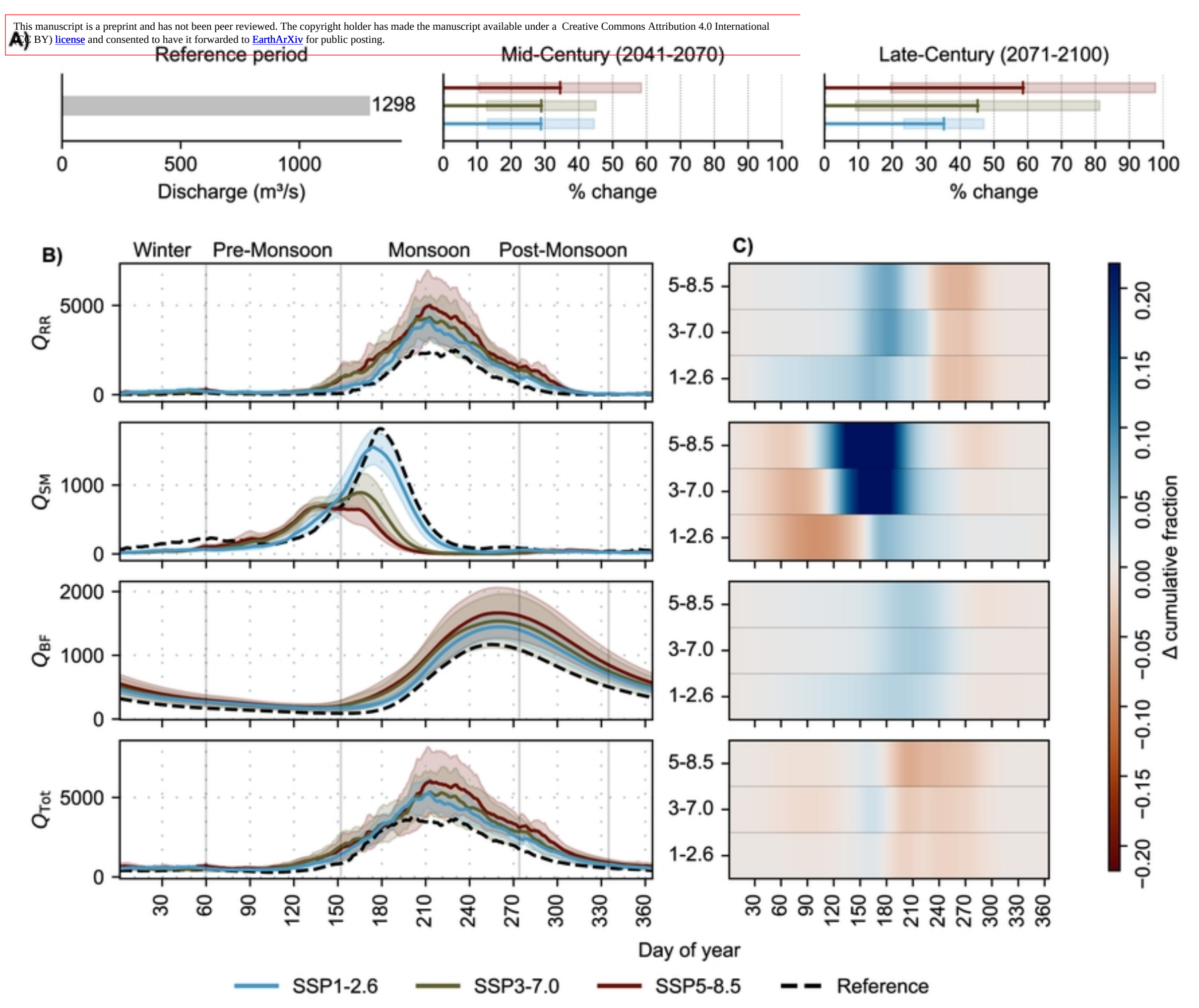


Fig 4

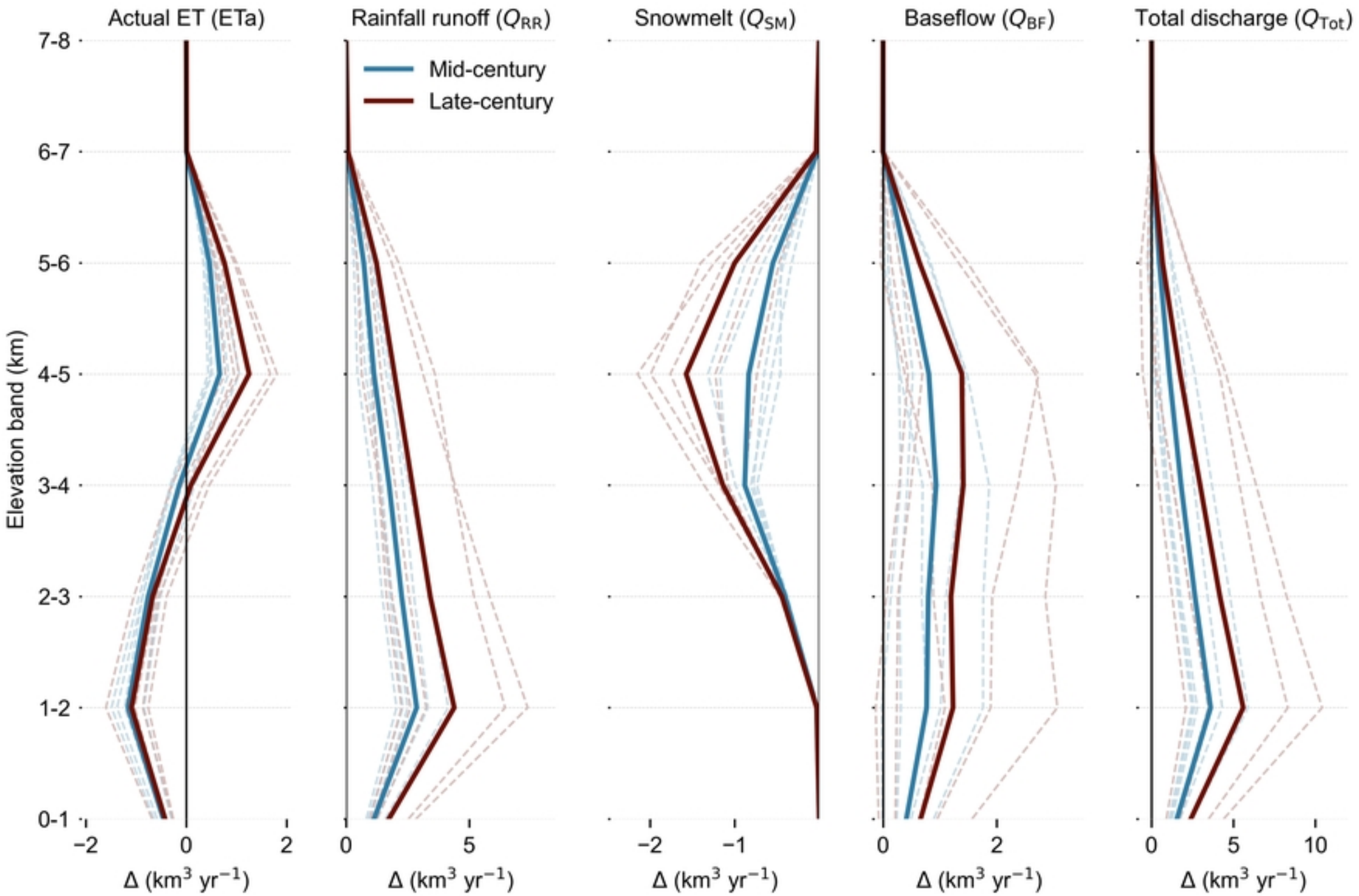
Actual ET (ETa)
Rainfall runoff ($Q_{RR}$)
Snowmelt ($Q_{SM}$)
Baseflow ($Q_{BF}$)
Total discharge ($Q_{Tot}$)
Mid-century
Late-century
Elevation band (km)
7-8
6-7
5-6
4-5
3-4
2-3
1-2
0-1
−2
0
2
0
5
−2
−1
0
2
0
5
10
Δ (km³ yr⁻¹)

Fig 5